34th Annual International Conference of the IEEE EMBS
San Diego, California USA, 28 August - 1 September, 2012

CFD Simulation of Hemodynamics in Sequential and Individual Coronary Bypass Grafts Based on Multislice CT Scan Datasets

Omid Hajati, Khalil Zarrabi, Reza Karimi and Azadeh Hajati

Abstract−**There is still controversy over the differences in the patency rates of the sequential and individual coronary artery bypass grafting (CABG) techniques. The purpose of this paper was to non-invasively evaluate hemodynamic parameters using complete 3D computational fluid dynamics (CFD) simulations of the sequential and the individual methods based on the patient-specific data extracted from computed tomography (CT) angiography. For CFD analysis, the geometric model of coronary arteries was reconstructed using an ECG-gated 64-detector row CT. Modeling the sequential and individual bypass grafting, this study simulates the flow from the aorta to the occluded posterior descending artery (PDA) and the posterior left ventricle (PLV) vessel with six coronary branches based on the physiologically measured inlet flow as the boundary condition.**

The maximum calculated wall shear stress (WSS) in the sequential and the individual models were estimated to be 35.1 N/m^2 and 36.5 N/m^2, respectively. Compared to the individual bypass method, the sequential graft has shown a higher velocity at the proximal segment and lower spatial wall shear stress gradient (SWSSG) due to the flow splitting caused by the side-to-side anastomosis. Simulated results combined with its surgical benefits including the requirement of shorter vein length and fewer anastomoses advocate the sequential method as a more favorable CABG method.

I. INTRODUCTION

There are two common surgical techniques for patients with multi vessel coronary disease: sequential and individual. According to the past researches, sequential saphenous vein graft (SSVG) has a better patency rate than individual saphenous vein grafts (ISVGs) in general [1,2]. In case of SSVG, a higher patency rate of the side-to-side anastomosis compared to the end-to-side anastomosis has been reported as well [3]. Intimal hyperplasia (IH) in the first year after surgery, and the formation and development of atherosclerosis in the years thereafter are probably causing the blockage of the graft and decreasing its patency rate. There are many factors that impact the initiation and progress of the anastomotic IH including: mismatch between the graft and the coronary artery, surgical injury, local hemodynamics and etc [4,5]. From the IH formation viewpoint, hemodynamic parameters include low wall shear stress (WSS), high WSS, large spatial wall shear stress gradient (SWSSG) and long residence time of blood cells [6,7,8,9,10,11]. 3D geometric reconstruction of coronary arteries and the estimation of the hemodynamic parameters distribution based on CFD modeling can be a non-invasive and an inexpensive solution to locate the IH and atherosclerosis risk areas. Most of the previously reported coronary artery bypass grafting (CABG) simulations have been limited to a subsection of the bypass grafts mainly the distal anastomosis [10,12]. Nevertheless, modeling a complete bypass including both proximal and distal anastomosis results in noticeably different velocity distribution as shown by Lee [13]. Sankaranarayanan et al. [14] investigated blood flow in aorta-left coronary bypass graft methods based on a simplified geometric model instead of a realistic patient-specific model. The results for the multiple bypass graft model have shown that compared to the sequential bypass graft model the peak magnitudes of the SWSSG are higher. In both models, the maximum WSS was observed at the toe of distal end-to-side anastomosis. In addition, a clinical study by Vural [1] implies a higher patency rate of sequential methods compared with that of an individual one. Despite a general inclination for sequential bypass grafting, there is no general consent regarding the optimal bypass grafting technique with the saphenous vein (SV) graft. As a result, the purpose of this work is to non-invasively evaluate hemodynamic parameters using complete 3D CFD simulations of the sequential and the individual methods based on the patient-specific data extracted from CT angiography for the first time and identify the optimal method.

II. METHODOLOGY

A. Computed tomography data acquisition

A 63 year old male patient with history of hypertension and typical chest pain underwent coronary CT angiography in TABA imaging center (Shiraz, Iran) by multislice CT scan (64-detector row scanner, GE VCT, USA) set at the following parameters: a detector collimation of 64×0.625 mm, the tube potential at 120 kV and a tube current of 678 mA. A bolus injection of 150 cc contrast (Iopromide, Ultravist 300) was followed by 30 cc saline solution via

Omid Hajati is with the Chemical Engineering Department, Shiraz University, Iran 71345 (corresponding author to provide phone: 98 (711) 625-6852; Fax: 98 (711) 625-6256852 e-mail: omid_hajati@yahoo.com)
Khalil Zarrabi is with the Cardiac Surgery Department, Shiraz University of Medical Sciences, Iran 71348 (email: zarrabisx@gmail.com)
Reza Karimi is with the Chemical Engineering Department, Shiraz University, Iran 71345 (email: ghkarimi@shirazu.ac.ir)
Azadeh Hajati is with the Radiology Department, Shiraz University of Medical Sciences, Iran 71348 (email: dr.azdhaj@yahoo.com

superficial vein. Synchronized to the electrocardiogram (ECG), the images were captured with slice thickness of 0.625 mm and the table feed of 7.2 mm/rotation. The period for each gantry rotation was about 0.35 s.

B. Geometric reconstruction

The 3D arteries model without any stenosis was reconstructed using ScanIP, a commercial package by Simpleware Ltd., employing a collection of digital images in DICOM format (276-slice). The blood arteries of interests were segmented semi-automatically combined with a manual segmentation to reconstruct small branches. Thresholding was performed as the first step of the segmentation to identify the dynamic range of the image pixels. Subsequently, portions of the patient's arteries, bones and other tissues which were non-relevant to the study were omitted. Afterwards, the inner wall surfaces of the arteries were covered by a triangular mesh using the marching cube algorithm. The final step of the reconstruction included the model smoothingwhich reduced the surface roughness. Figure 1a depicts one of the original CT-scan images in which all the pixels within the specified dynamic range are highlighted. The final reconstructed model is shown in Figure 1b where the arteries of interest can be seen.

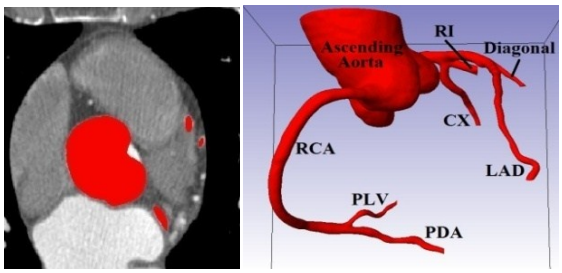

Figure 1A single slice of the original CT-scan data with the highlighted dynamic range (left) and the reconstructed model of the coronary arteries (right).

The extracted volumeswere imported into the pre-processing GAMBIT package. Two 90% stenoses were implemented at the posterior descending artery (PDA) and the posterior left ventricle (PLV) in the proximity of the right coronary artery (RCA) bifurcation. SV grafts were subsequently added to both sequential and individual models (Figure 2).

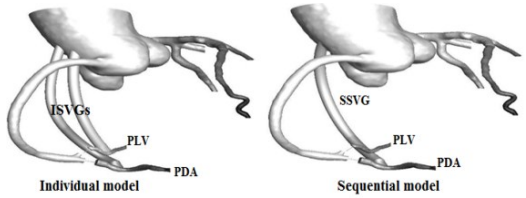

Figure 2 Created Individual and Sequential Bypass Methods

The mean diameter, length, and the location of the SV's suture are realistic and based on surgical observation (Figure 3). Due to the deformation of the larger diameter graft sutured to the smaller vessel as observed in the surgery, the intersection between the graft and the host artery has an elliptical shape. The curvature of the grafts has been considered in such a way to overlay them perfectly over the heart. All these points have been considered in the present study.

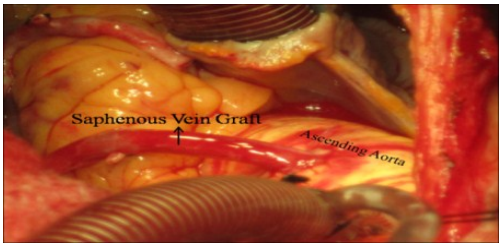

Figure 3 Surgical Observation of SV Grafting

The corresponding models were subsequently meshed and the mesh quality was further improved by applying various size functions across the model. The anatomy of coronary arteries is very complex and can only be reconstructed by an unstructured meshing. Tetrahedral elements were used in this study and about 2,002,000 elements were selected as the optimal meshing size. The average and maximum equiangle skew and equisize skew of the meshing were about 0.3 and 0.78, respectively which implies a high mesh quality.

C. Model assumptions and boundary conditions

Coronary arteries branches that have been modeled in this study include: left anterior descending (LAD), major diagonal, proximal of circumflex (CX) and ramus intermedius (RI), PDA and PLV. Although the RI artery exists in only one third of patients [16], the studied patient had an abnormally large one. This study simulated the mid-diastole point (t =0.58 s) at which the aortic valve is fully closed and there is a maximum perfusion in the coronary arteries. A uniform inlet flow was assumed in the proximal part of ascending aorta. The velocity profile was estimated based on the flow rate waveforms in the cardiac cycle [17,18]. In this model, the flow through the six outlets was based on Murray law [19] (outflow boundary condition). The blood flow was modeled as a 3D, steady-state, incompressible and laminar flow considering the Reynold's number of about 300 in the small arteries.Newtonian flow can approximate the effect of the blood viscosity well in case of medium to high average shear rates [20]. Therefore, the blood was modeled as a Newtonian fluid with the viscosity and the density of 0.0035 Pa.s and 1060 Kg/m^3, respectively. Walls were modeled as rigid and impermeable and no-slip boundary condition was applied at the walls.

D. Computational fluid dynamics

The mesh data and the boundary conditions specified in GAMBIT were imported into the main CFD solver FLUENT. A numerical code solved the flow governing equations; continuity and momentum equations as follows:

$$\nabla \cdot \boldsymbol{v} = 0 \quad (1)$$

$$\rho \boldsymbol{v} \cdot \nabla \boldsymbol{v} = -\nabla \cdot \boldsymbol{\tau} - \nabla P \quad (2)$$

In these equations, **v**, P, ρ and $\boldsymbol{\tau}$ are the velocity vector, the pressure, the density and the shear stress tensor, respectively. Implicit formulation was used to linearize the equations which were then solved by the segregated method. SIMPLE technique was chosen as the pressure-velocity coupling and the pressure and the momentum were descritized by the first order and the second order discretization, respectively. A node-based gradient evaluation is more accurate than cell-based schemes for unstructured meshes and as a result, green-gauss node-based method was used to evaluate the gradients. Convergence criterion was met when the residuals of velocity components reduced below 10^{-5} which typically takes place after 1200 iterations.

III. RESULTS AND DISCUSSION

The aortic valve is fully closed at the mid-diastole point and the back flow perfuses primarily the left main coronary artery (LMCA) through the ascending aorta and partly enters the grafts. Combining the conservation of mass and the Murray law [18] indicates that approximately 67.7% of the back flow from the ascending aorta enters the LMCA. The corresponding blood flow is distributed among branches of the CX, major diagonal, the distal part of the LAD and RI at 16.8%, 21.7%, 24.4% and 37.1% rates, respectively. The large flow through the RI artery is attributed to its unusually large diameter in the patient. A negligible flow is permitted into the distal end of PDA and the PLV by the RCA as a result of the 90% stenosis at their proximal portions. Consequently, the grafts supply the majority of the flow in the distal branches of PDA and PLV. 66.1% of the grafts input flow is streamed into the PDA and the remaining to the PLV.Along the grafts, the blood flow is skewed and peaks near the outer wall of the grafts.Figure 4 depicts the simulated velocity profile at various cross-sections along the grafts. Figure 5 compares the maximum velocity values along the lengths of the investigated grafts. As evident from this figure, a higher velocity is observed at the proximal segment in case of the sequential graft (~34 cm/s) in comparison with the individual bypass grafts (~22 cm/s and 11 cm/s). The sudden increase in the velocity at the end of the grafts is due to the deformation of the larger diameter graft sutured to the smaller vessel. In contrast, the blood velocity decreases at the bridge portion of the sequential graft as a result of the flow division to the PDA artery through the side-to-side anastomosis.

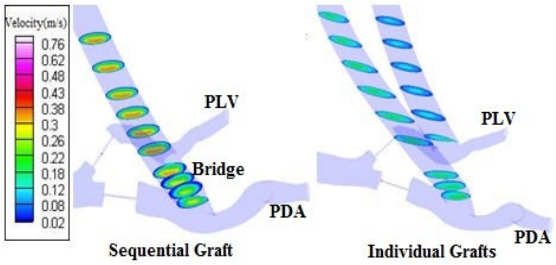

Figure 4 Simulated blood velocity profiles in sequential and individual grafts. proximal segment of the sequential graft showed higher velocity in comparison with that in the individual grafts.

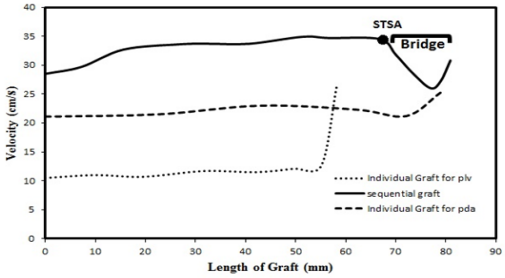

Figure 5 Comparison of the maximum velocity along the studied grafts: sequential graft provides a significantly greater blood velocity in comparison with the individual grafts

Malek et al. [21] have shown that the proatherogenic endothelial phenotype and the endothelial quiescence are stimulated at WSS values below 0.4 N/m^2 and above 1.5 N/m^2, respectively. WSS of higher than 10 N/m^2 may causetheendothelial disruption which could lead to atherosclerosis.

Peak WSS is seen at the toe of the individual end-to-side anastomosis. Other regions that experience high WSS are the distal ends of the LAD which may be attributed to the tapering of the vessels. This study states that at any flow divider, the low WSS prevails at the walls opposite the junction. On the contrary, the values of the WSS at the flow divider are most probably exerting a protecting role on the endothelium. The negligible flow at the proximal portion of the PDA and the PLV results in very low WSS and insignificant WSS variations. In addition, almost no shear stress can be seen at the heel and on the bed across from it. In both models, strong variations in the WSS can be seen in the anastomotic region and the maximum WSS values are estimated to be 35.1 N/m^2 and 36.5 N/m^2 in the sequential and the individual models, respectively (Figure 6).

A better graft patency may be contributed to a uniform hemodynamic environment caused by the low SWSSG associated with a uniform flow. A high SWSSG stimulates IH, atherosclerosis and thrombosis and a threshold of

25000 N/m^3 has been suggested by Lei et al [22] as the critical SWSSG value.

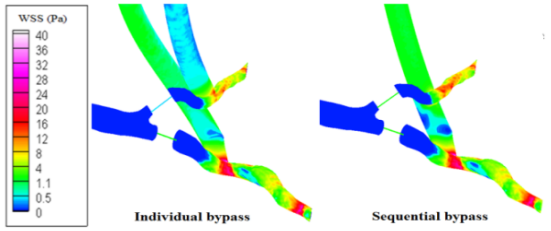

Figure 6 The simulated contour plots for WSS in the Sequential and the Individual bypass methods. The WSS in the toe of end-to-side anastomosis is 35.1 N/m^2 and 36.5 N/m^2 in the sequential and the individual models, respectively.

The maximum value of SWSSG in the side-to-side anastomosis in the sequential model is calculated to be 12124 N/m^3 while this parameter in the toe of the graft-PLV junction in individual grafts is around 40000 N/m^3. Also high SWSSG values are observed at the toe of the most distal anastomosis in both models. In the sequential bypass graft model, lower SWSSG values are obtained in comparison with the individual bypass graft model (Figure 7).

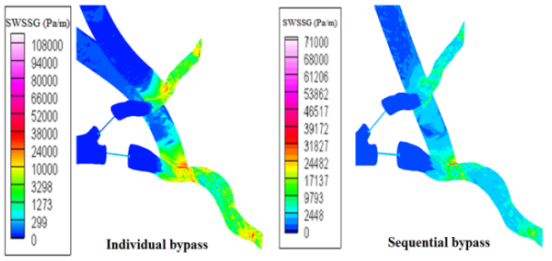

Figure 7 The simulated contour plots for SWSSG in the Sequential and the Individual bypass methods. lower SWSSG values are achieved in sequential model.

The side-to-side anastomosis which is exclusive to the sequential model causes a flow splitting which induces a well-distributed velocity profile at the bridge section and improves the WSS distribution. The side-to-side anastomosis has a smoother flow with smaller spatial gradients of WSS as compared to the end-to-side anastomosis. In this modeling, the vein length for two bypasses in SSVG was 58% of the length of the ISVGs which translates into a complete revascularization with a shorter vein segment. Considering the fewer anastomoses requirement, the sequential bypass has shorter operation time in comparison with the individual bypass.

IV. CONCLUSION

In summary, we have presented novel CT-based models for two CABG techniques. We conclude that the sequential grafting results in more favorable hemodynamic parameters that correlate with lowering the risk of restenosis and IH development. Consequently, these findings suggest that the sequential bypass grafting is more favorable than the individual type at least in theory.

REFERENCES

[1] Vural KM, Sener E, Tasdemir O. Long-term patency of sequential and individual saphenous vein coronary bypass grafts. *Eur J CardiothoracSurg*, vol. 19, pp. 140–144, 2001.

[2] Kim HJ, Lee TY, Kim JB, Cho WC, Jung SH, Chung CH et al. The impact of sequential versus single anastomoses on flow characteristics and mid-term patency of saphenous vein grafts in coronary bypass grafting. *J ThoracCardiovascSurg*, vol. 141, pp. 750-754, 2011.

[3] Kieser TM, FitzGibbon GM, Keon WJ. Sequential coronary bypass grafts. Long-term follow-up. *J ThoracCardiovascSurg*, vol. 91, pp. 767-772, 1986.

[4] Mullany CJ. Coronary artery bypass surgery. *Circulation*, vol. 107,pp. 21–22, 2003.

[5] Abbott WM, Megerman J. Does compliance mismatch alone cause neointimal hyperplasia? *J VascSurg*, vol. 9, pp. 507, 1989.

[6] Ethier CR. Computational modeling of mass transfer and links to atherosclerosis. *Ann Biomed Eng,* vol. 30, pp. 461–471, 2002.

[7] Ku DN, Giddens DP, Zarins CK, Glagov S. Pulsatile flow and atherosclerosis in the human carotid bifurcation. Positive correlation between plaque location and low oscillating shear stress. *Arteriosclerosis*, vol. 5, pp. 293–302, 1985.

[8] Friedman MH, Bargeron CB, Duncan DD, Hutchins GM, Mark FF. Effects of arterial compliance and non-Newtonian rheology on correlations between intimal thickness and wall shear. *J BiomechEng*, vol. 114, pp. 317-320, 1992.

[9] Fry DL. Certain histological and chemical responses of the vascular interface to acutely induced mechanical stress in the aorta of the dog. *Circ Res,* vol. 24, pp. 93-108, 1969.

[10] Ojha M, Ethier CR, Johnston KW, Cobbold RS. Steady and Pulsatile Flow Fields in an End-to-Side Arterial Anastomosis Model. *J VascSurg*, vol. 12, pp. 747–753, 1990.

[11] Bassiouny HS, White S, Glagov S, Choi E, Giddens DP, Zarins CK. Anastomotic Intimal Hyperplasia: Mechanical Injury or Flow Induced. *J VascSurg*, vol. 15, pp. 708–717, 1992.

[12] Frauenfelder T, Boutsianis E, Schertler T, Husmann L, Leschka S, Poulikakos D et al. Flow and wall shear stress in end-to-side and side-to-side anastomosis of venous coronary artery bypass grafts. *Biomed Eng Online*, vol. 6, pp. 35, 2007

[13] Lee D, Su JM, Liang HY. A numerical simulation of steady flow fields in a bypass tube. *J Biomech*, vol. 34, pp. 1407–1416, 2001.

[14] Sankaranarayanan M, Ghista DN, Chua LP, Tan YS, Sundaravadivelu K, Kassab GS. Blood flow in an out-of-plane aorto-left coronary sequential bypass graft. In: Guccione JM, Kassab GS, Ratcliffe M. Computational Cardiovascular Mechanics: Modeling and Applications in Heart Failure. New York: Springer-Verlag, 2010.

[15] Lorensen WE, Cline HE. Marching cubes: a high-resolution 3D surface construction algorithm. *Comput Graph* , vol. 21, pp. 63–169, 1987.

[16] Haaga JR. CT and MRI of the whole body. 5TH ed. Vol.1. MOSBY. 2009:1133-1134.

[17] Ganong WF. Review of Medical Physiology, Appleton & Lange, Norwalk, Conn., 1999.

[18] Sankaranarayanan M, Ghista DN, Poh CL, Seng TY, Kassab GS. Analysis of blood flow in an out-of-plane CABG model. *Am J Physiol Heart CircPhysiol*, vol. 291, pp. H283–95, 2006.

[19] Murray CD. The physiological principle of minimum work. I. The vascular system and the cost of blood volume. *ProcNatlAcadSci*, vol. 12, pp. 207-214, 1926.

[20] Johnston BM, Johnston PR, Corney S, Kilpatrick D. Non-Newtonian blood flow in human right coronary arteries: steady state simulations. *J Biomech*, vol. 37, pp. 709-720, 2004.

[21] Malek AM, Alper SL, Izumo S. Hemodynamic shear stress and its role in atherosclerosis. *J Am Med Assoc,* vol. 282, pp. 2035–2042, 1999.

[22] Lei, M, Kleinstreuer C, Truskey GA. A focal stress gradient-dependent mass transfer mechanism for atherogenesis in branching arteries. *Med. Eng. Phys.* 18, pp. 326–332, 1996.